JCTC Journal of Chemical Theory and Computation

ARTICLE

pubs.acs.org/JCTC

On the Intramolecular Hydrogen Bond in Solution: Car−Parrinello and Path Integral Molecular Dynamics Perspective

Przemyslaw Dopieralski,*[,†] Charles L. Perrin,*[,‡] and Zdzislaw Latajka[†]

[†]Faculty of Chemistry, University of Wroclaw, Joliot−Curie 14, 50-383 Wroclaw, Poland

[‡]Department of Chemistry and Biochemistry, University of California at San Diego, La Jolla, California 92093-0358, United States

Supporting Information

ABSTRACT: The issue of the symmetry of short, low-barrier hydrogen bonds in solution is addressed here with advanced ab initio simulations of a hydrogen maleate anion in different environments, starting with the isolated anion, going through two crystal structures (sodium and potassium salts), then to an aqueous solution, and finally in the presence of counterions. By Car−Parrinello and path integral molecular dynamics simulations, it is demonstrated that the position of the proton in the intramolecular hydrogen bond of an aqueous hydrogen maleate anion is entirely related to the solvation pattern around the oxygen atoms of the intramolecular hydrogen bond. In particular, this anion has an asymmetric hydrogen bond, with the proton always located on the oxygen atom that is less solvated, owing to the instantaneous solvation environment. Simulations of water solutions of hydrogen maleate ion with two different counterions, K^+ and Na^+, surprisingly show that the intramolecular hydrogen-bond potential in the case of the Na^+ salt is always asymmetric, regardless of the hydrogen bonds to water, whereas for the K^+ salt, the potential for H motion depends on the location of the K^+. It is proposed that repulsion by the larger and more hydrated K^+ is weaker than that by Na^+ and competitive with solvation by water.

1. INTRODUCTION

Today no one will deny that hydrogen bonds (H-bonds) are a key feature of molecular structure and reactivity.[1−11] Despite the fact that an enormous amount of experimental and theoretical work has been devoted to unveiling their peculiar character in the past decade, H-bonds are still a rich source of new and old challenging, unsolved problems.

One of those problems is the symmetry of short, low-barrier H-bonds in solution.[12] For many years it was hoped that the crystal structure would describe a molecule in solution. Yet crystal structures of the same H-bond can differ. For example, the potassium salt of hydrogen maleate (Hmaleate) shows a centered hydrogen,[13] whereas the hydrogen is asymmetrically positioned in the corresponding sodium salt.[14] Nevertheless, NMR studies showed that those H-bonds are invariably asymmetric in aqueous solution.[15,16] It was initially proposed that the asymmetry is a consequence of the polarity of water, which stabilizes the localized negative charge of O−H···O^- or $^-$O···H−O more than the delocalized one of $(O\cdots H\cdots O)^-$.[17] This rationale was supported by computer simulations.[18] However, further NMR studies in nonpolar organic solvents continued to show asymmetric H-bonds,[19] even in the NHN H-bonds of protonated 1,8−bis(dimethylamino)naphthalenes,[20] in nonionic species,[21] in a zwitterion,[22] in the intermolecular H-bond of pyridine−dichloroacetic acid complexes,[23] and in the "strongest" of H-bonds.[24] Therefore it was concluded that although the environments around the two carboxyl groups can be identical in a crystal, a solution is disorganized, with one of the carboxyls instantaneously solvated better than the other,[25] leading to the presence of equilibrating solvatomers (isomers, stereoisomers, or tautomers that differ in solvation).[22] QM/MM calculations (AM1-SRP/AMBER) on hydrogen phthalate anion in solution support this interpretation.[26] Moreover, the absence of symmetric H-bonds in solution suggests that they have no special stabilization.[27]

An early theoretical study on the simplest case, the isolated Hmaleate anion, found the potential for the proton transfer to be a double minimum (C_s symmetry), with a barrier height of 1.4 kcal/mol and with a structure of C_{2v} symmetry being a transition state.[28] Later studies confirmed the asymmetric structure as more stable, although the barrier varies from 0.1 kcal/mol up to a few kcal/mol, depending on the method used.[29−33] Plane-wave DFT calculations found a broad, flat potential energy surface for the unit cell but returned to a shallow double-well surface when the crystal packing forces were removed.[34,35] Thus, questions dealing with the symmetry of Hmaleate anion are still discussed.

Here we use both ab initio Car−Parrinello molecular dynamics (CPMD) simulations and fully quantum mechanical path integral molecular dynamics (PIMD) on aqueous Hmaleate ion at 298 K to provide a theoretical understanding of how the solvent and the counterions K^+ and Na^+ modify the symmetry of the intramolecular H-bond. Based on a new procedure, which distinguishes separate free-energy profiles for those periods during the simulation when oxygen atoms of the intramolecular H-bond are solvated to different or similar extents, we can discover the determinants of the H-bond symmetry and confirm some intriguing experimental findings by Perrin et al.[19]

2. RESULTS AND DISCUSSION

2.1. Isolated Hydrogen Maleate Ion and Its Potassium and Sodium Salts. Before addressing the main theme, one must

Received: August 19, 2011
Published: October 10, 2011

dx.doi.org/10.1021/ct200580c | J. Chem. Theory Comput. 2011, 7, 3505−3513

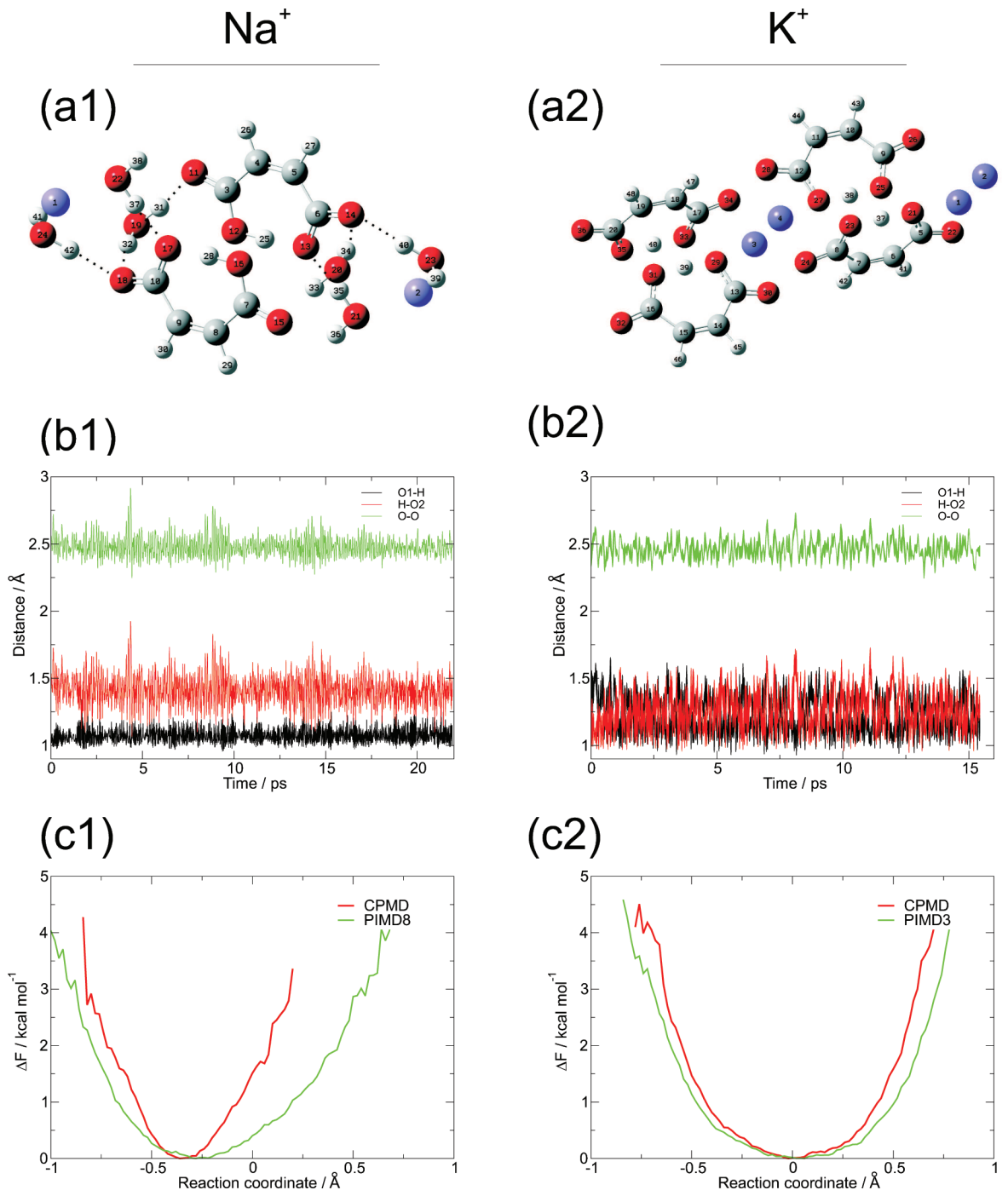

Figure 1. Two crystal structures of Hmaleate salts from CPMD and PIMD simulations: sodium (left panel: a1, b1, and c1) and potassium (right panel: a2, b2, and c2). (a1,b1) Representative snapshot of the crystal unit cell. (b1,b2) Time evolution of the distances involved in the intramolecular H-bond. (c1,c2) Free-energy profiles for proton transfer within the H-bond.

consider the isolated Hmaleate ion and the crystal structures of its salts. To confirm that the isolated ion represents a situation with a truly symmetric-centered single, well potential or, equivalently, a double well with a low barrier, CPMD and PIMD room temperature simulations have been performed. Additionally we have performed CPMD and PIMD simulations for sodium and potassium Hmaleate crystals.

The results for the isolated ion show the O···O distance to be 2.457 Å, and both O···H distances are the same, 1.235 Å. Calculated structures of sodium and potassium Hmaleate crystals, shown in Figure 1a1 and a2, reproduce the experimental structures. In particular, the sodium salt shows a low symmetry and an asymmetric H-bond, whereas the potassium salt is a highly symmetric crystal, with a centered proton. However, it must be noted that although the potassium crystal is truly a high-symmetry one, in the sodium crystal the presence of water molecules reduces the symmetry and is responsible for different environments of the two oxygen atoms involved in the intramolecular H-bond of Hmaleate.

dx.doi.org/10.1021/ct200580c |J. Chem. Theory Comput. 2011, 7, 3505–3513

Table 1. Time-Averaged Intramolecular H-bond Distances from Calculations on Sodium and Potassium Hmaleate Salts

	NaHMal			KHMal	
bond	CPMD	PIMD8	expt[14]	CPMD	expt[36]
O−H	1.08	1.13	1.079	1.22	–
H···O	1.41	1.37	1.369	1.23	–
O···O	2.48	2.47	2.445	2.44	2.434

Time-averaged H-bond distances for these two simulations have been collected in Table 1, and instantaneous distances are displayed in Figure 1b1 and b2 .

The graph in Figure 1b1 shows the results from simulations on the crystal structure of sodium Hmaleate. As expected, the O−O distance shows little variation, and this behavior is maintained in all the subsequent simulations. In this crystal one O−H distance remains short, near 1.0 Å, while the other is longer, near 1.4 Å, but with greater variability. This leads to a highly asymmetric single-well potential for proton motion within the H-bond, as shown in Figure 1c1. In this crystal the proton is not able to jump from one oxygen atom to the other within the intramolecular H-bond because the two oxygens are in different molecular environments. By inspection of the structure, it can be seen that one of the oxygens is closer to its nearest sodium than the other oxygen is to its closest sodium. The difference is approximately 1 Å. Additionally, the oxygen that has the closer sodium ion participates in a H-bond to the H of a water molecule, whereas the other oxygen does not coordinate any water molecules. Thus, because of crystal packing, which produces an inequivalence of the two oxygens, an asymmetric single-well potential for proton motion within the H-bond is induced, as presented in Figure 1c1, with the proton located on the oxygen that is farther from the sodium ion and that lacks a water of solvation. Inclusion of quantum effects by the PIMD treatment does not qualitatively change the results, and the potential remains an asymmetric single well but with larger fluctuations of the proton motion, as included in Figure 1c1.

For the potassium Hmaleate crystal, the situation is different. The graph in Figure 1b2 shows the results of the simulations. In this crystal both O−H distances vary rapidly but stay near 1.2 ± 0.1 Å. This leads to a broad and symmetric single-well potential for proton motion within the H-bond, as shown in Figure 1c2. Both the X-ray crystal structure and our simulations show that a chain, $\cdots K^+ \cdots O1-H-O2 \cdots K^+ \cdots$, is observed, with the potassium ions placed symmetrically, at equal distances, with respect to both oxygens. Because each oxygen atom has exactly the same neighborhood, the proton is located most of the time in the center of the H-bond, as shown in Figure 1b2, and the potential is a symmetric single-well one, as depicted in Figure 1c2. The result from PIMD simulations is also shown in Figure 1c2. The inclusion of quantum effects does not change the picture, as expected.

2.2. Hydrogen Maleate Ion in Water. In Figure 2 the results from CPMD and PIMD simulations on aqueous Hmaleate anion are collected. The graph in Figure 2b1 shows that according to CPMD, the proton jumps from one oxygen to the other, with an average residence time of around 1 ps but sometimes longer. The proton is found more often on O1. These proton positions correspond to an asymmetric double-well potential (Figure 2c1) with a barrier height around 1 kcal/mol. This is likely to be a consequence of the instantaneous solvation environment, which favors one solvatomer over another.

We have probed solvation in more detail by summing the number of H-bonds between the hydrogen atoms of the surrounding waters and each of the two oxygen atoms in the intramolecular H-bond of the Hmaleate anion. The distance dependence for deciding to include a H-bond was investigated and was finally taken as 2.5 Å. Based on this routine, we find that oxygen atom O1 has been less solvated than O2 (with fewer H-bonds from water molecules) for approximately 48.2% of the simulation time, O2 has been less solvated than O1 for 15.1% of the time, and both oxygen atoms have been solvated similarly during approximately 26.7% of the time.

Moreover, the position of the proton in the intramolecular H-bond is correlated with the relative solvation of the two Hmaleate oxygen atoms. The remarkable result is that the proton is always located on the oxygen that is less well solvated.

This result, and other considerations presented here, bring to mind a picture of donor and acceptor solvation theory similar to the Marcus theory of electron transfer.[37] Proton or electron movement (but not the proton or electron transfer itself) is much faster than reorganization of the solvent, assumed in Marcus theory. However, we cannot assume that the donor and acceptor moieties are only weakly coupled—this assumption of Marcus would not be true in Hmaleate anion. Marcus theory depicts electron transfer as made possible by prearrangement of fluctuating solvent molecules. When, by chance, such a correct arrangement happens, the transfer can take place. Our observation is very similar. The proton is always located on the oxygen that is less well solvated; using the Marcus idea, we can reverse this statement and say that the less well solvated oxygen atom is preferred to possess the proton, and the better solvated oxygen is preferred as the bearer of more negative charge, making it a future acceptor. When by chance this solvation pattern is reversed by solvent fluctuations, the proton can jump. These ideas were exploited in studies by Borgis and Hynes[38] and by Mavri et al.[39] However, the time frame of the CPMD simulations and the nature of delocalized plane-wave basis set do not allow us to use directly the methodologies described there.

These results suggest that the asymmetric double-well potential and the apparent barrier of 1 kcal/mol in Figure 2c1 are a consequence of averaging over instantaneous solvation environments that sometimes favor one solvatomer and then the other. Indeed, if the averaging is restricted to shorter time intervals, a different picture emerges. The separate free-energy profiles for the 48.2% of the simulation time when O1 was less solvated than O2, for the 15.1% of the time when O2 was less solvated than O1, and for the 26.7% of time when both oxygen atoms were solvated similarly are shown in Figure 3a1. For the first two cases, where the two oxygens were solvated to different extents, the free-energy profile becomes a single-well potential, with its minimum at the oxygen that is less solvated. There is no longer a minimum at the other, better-solvated oxygen. For the third case, where both oxygen atoms were solvated similarly, the free-energy profile remains a double-well potential, as in the earlier Figure 2c1, with nearly the same difference in well depths, but the barrier has become indistinct. Thus these profiles in Figure 3a1 show how the instantaneous potential responds to the solvation environment. An important conclusion is that the apparent barrier in the CPMD simulations is an artifact of the long-term averaging over different solvation environments.

One must be aware of the fact that the free energies presented in Figures 3 and 5 below are not in a sense the most rigorously defined ones. Definition of a free energy profile requires a

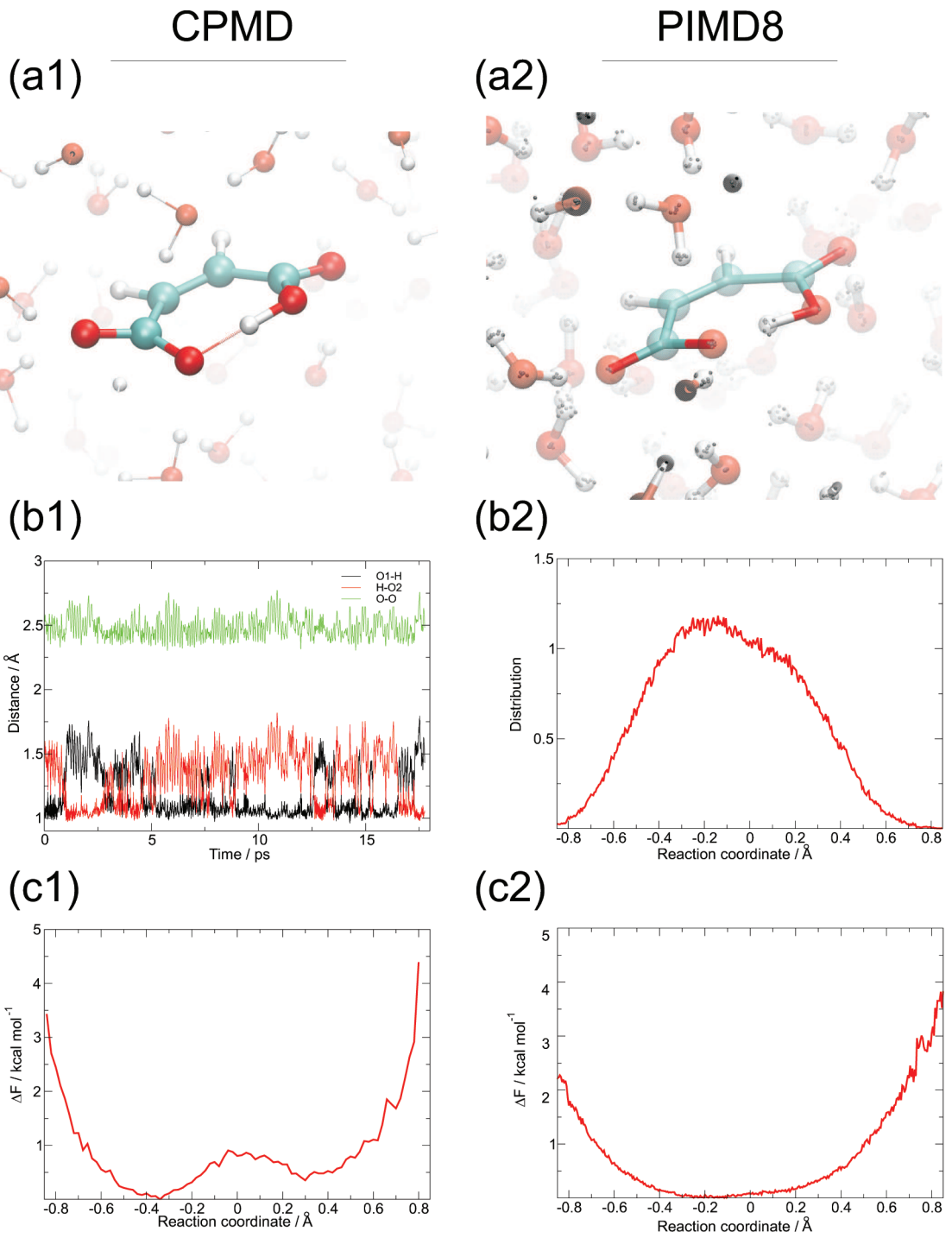

Figure 2. Hmaleate ion in water from CPMD (left column: a1, b1, and c1) and from PIMD (right column: a2, b2, and c2). (a1,a2) Representative snapshot from simulations, for PIMD the replicas of each atom as small gray spheres are marked. (b1) Time evolution of the distances involved in the intramolecular H-bond. (b2) Distribution function for the reaction coordinate (c1,c2) Free energy profiles for proton transfer within the H-bond.

complete phase-space average over all orthogonal coordinates, so our averaging cannot yield a proper free energy. Nevertheless our projections/averaging of "free energies" are still reasonable approximations and are able to capture the correlation between proton localization in the H-bond and the local solvation pattern. However, it is not possible to analyze energetics based on these figures. A more rigorous way to define the free energy is to introduce a second reaction coordinate (as was done by Tuckerman for OH^- solvation),[40] which in our case is the difference in hydration number of oxygen atoms involved in the H-bond. For figures and more details see Supporting Information.

According to PIMD simulation, the situation is slightly different. Figure 2b2 shows the distribution of the reaction coordinate, and Figure 2b3 shows the corresponding free-energy profile. Because of the quantum character of the proton there is no energy barrier associated with proton transfer, and a slightly

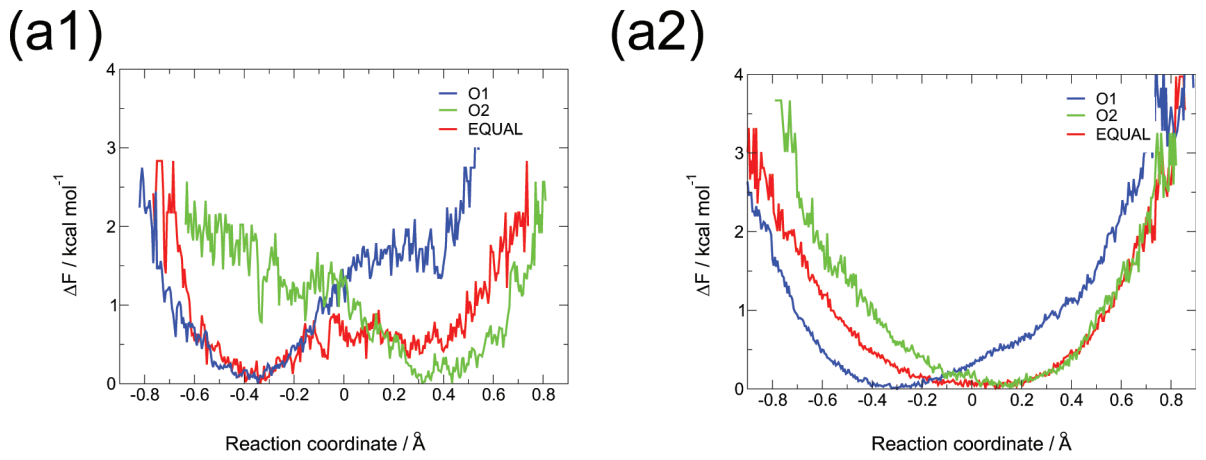

Figure 3. Free-energy profiles for H motion in aqueous Hmaleate ion from CPMD (a1) and from PIMD (a2) separately for the simulation time when O1 was less solvated than O2, for the time when O2 was less solvated than O1, and for the time when both oxygen atoms were solvated similarly.

asymmetric single-well potential is observed, with the proton located predominantly on one oxygen atom of Hmaleate.

As previously, we have quantified the solvation and find that for the first 6 ps of simulation time one oxygen atom (designated O1) continued to be less solvated than the other, thereby favoring one solvatomer. Afterward O2 is sometimes less solvated, so that the other solvatomer becomes favored. But there is no possibility of a single centered potential. More specifically, population analysis shows that for approximately 44.6% of the simulation time oxygen atom O1 was less solvated than oxygen O2 and for 16.5% of the time oxygen atom O2 was less solvated. For approximately 38.9% of the time both oxygen atoms in the H-bond were solvated more or less the same.

However, the slightly asymmetric single-well potential of Figure 2c2, with the proton apparently located on oxygen that is less well solvated, is again a consequence of averaging over instantaneous solvation environments. If the averaging is restricted to shorter time intervals, a different picture emerges. The separate free-energy profiles for the 44.6% of the simulation time when O1 was less solvated than O2, for the 16.5% of the time when O2 was less solvated than O1, and for the 38.9% of time when both oxygen atoms were solvated similarly are shown in Figure 3a2. For the first two cases, where one oxygen was less solvated than the other, the slightly asymmetric single-well potential is no longer restricted to one in which the proton is located on O1. Instead, the proton is located on the oxygen that is less solvated. Moreover, for the 38.9% of time when both oxygen atoms were solvated to nearly the same extent, the single well is no longer asymmetric but is symmetric, within the accuracy of the sampling. Thus these profiles show how the instantaneous potential responds to the solvation environment. A further conclusion is that the strong asymmetry in the distribution function and the free-energy profile of Figure 2b2, c2 is a result of the long-term averaging over solvation environments, during most of which O1 happens to be less well solvated.

Thus we have shown that the intramolecular H-bond in Hmaleate ion in water has an asymmetric H-bond owing to the instantaneous solvation environment. In principle, with sampling over a longer time, the oxygens must become equivalent, restoring an apparent symmetry between them. Under such circumstances, the total time during which O1 is better solvated than O2 must be equal to the total time during which O2 is better solvated than O1, along with times during which they are solvated equally. However, the simulation time that we used was too short to permit the oxygens to become equivalent. The instantaneous asymmetry of the H-bond then reflects the instantaneous solvation environment.

2.3. Counterion Effects. We next consider the influence of counterions on H-bond symmetry. We have examined two counterions, sodium and potassium, for which crystal structures have been discussed in the Isolated Hydrogen Maleate Ion and Its Potassium and Sodium Salts Section. The presence of a counterion is a major factor that can stabilize an asymmetric structure. According to Lluch's calculations on the QM/MM level (AM1-SRP/AMBER) for the H-bond in the potassium salt of Hphthalate anion in chloroform, the energy profile for the intramolecular proton transfer along the H-bond is a double well with two equivalent asymmetric minima.[26] Those calculations show further that a transition state with a centered position of the proton is observed when potassium ion is equidistant to both oxygen atoms of the H-bond and that an energy minimum is observed when the potassium ion is equidistant to the two oxygen atoms of one carboxyl group.

Results of our CPMD and PIMD simulations are presented in Figure 4. At the beginning of the simulations a bare Na^+ or K^+ was placed equidistant to the two oxygens of one of the carboxylates. During the equilibration period, 4.0 water molecules hydrate the Na^+ and 6.4 waters hydrate the K^+. However, there are no waters directly between either M^+ and the anion, because the equilibration and the simulation times are too short to overcome the barrier to separating the ions sufficiently to permit water to insert between them. In principle, the simulations could have been extended to much longer times or could have been started with fully hydrated $Na^+(H_2O)_5$ or $K^+(H_2O)_6$ near the Hmaleate anion, but this would be less interesting because the influence of the M^+ would be smaller and would exert less control on the H-bond.

Figure 4a1 and a2 shows the spatial distribution functions of the Na^+ and K^+ in the vicinity of Hmaleate anion. The figures reveal differences in the positioning of sodium and potassium ions around the carboxyl group. Most of the time the sodium ion was located equidistant to the two oxygen atoms of one carboxyl, whereas the potassium ion tended to stay closer to the oxygen atom that is involved in the intramolecular H-bond. Figure 4b1 and b2 shows further how the position of the hydrogen in the H-bond varies during the simulations. Figure 4c1 and c2 show the resulting free-energy profiles for motion of the hydrogen.

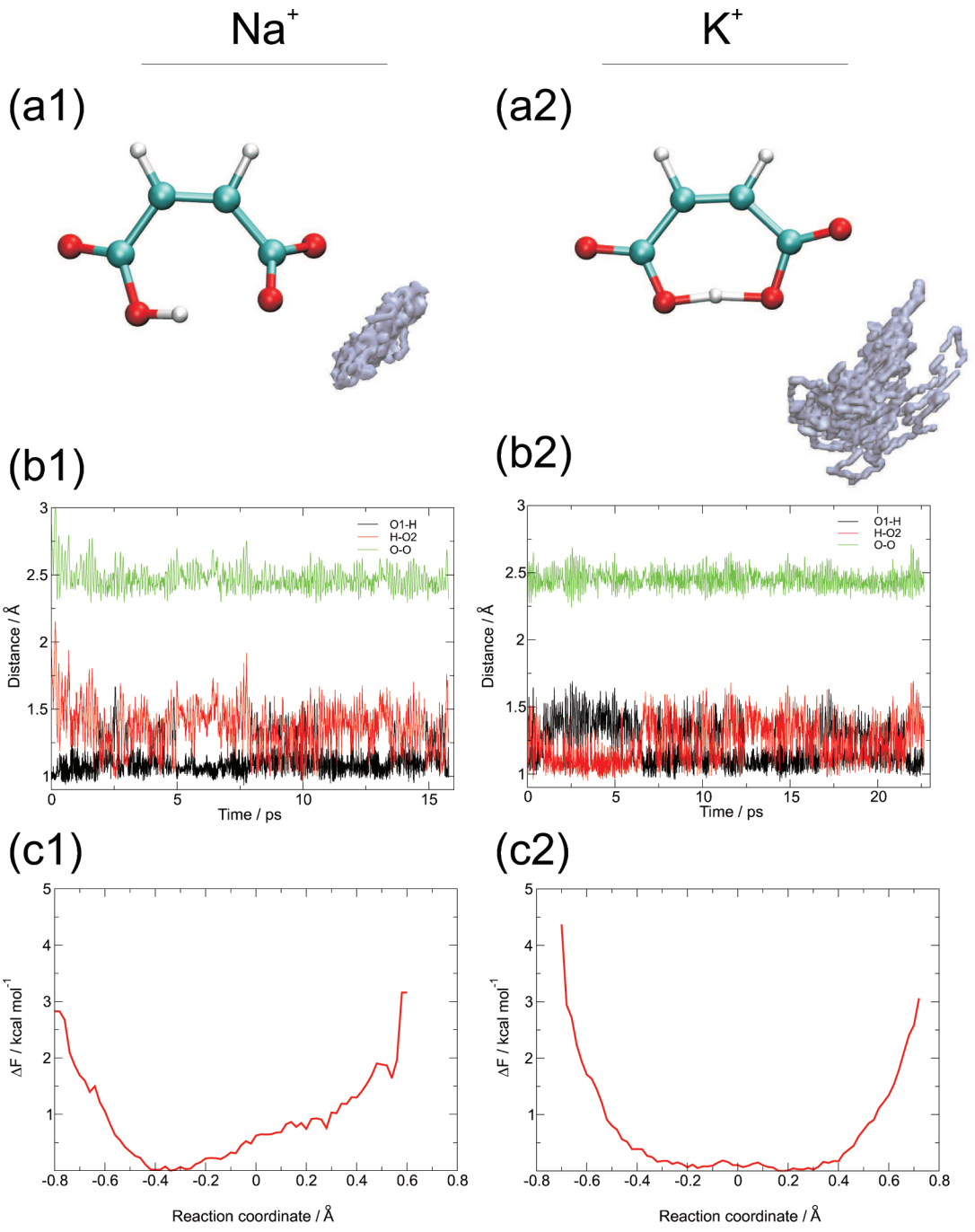

Figure 4. Hmaleate ion in water from CPMD simulations with two different counterions: sodium (left panel: a1, b1, and c1) and potassium (right panel: a2, b2, and c2). (a1,a2) Spatial distribution function of the counterion around Hmaleate ion. (b1,b2) Time evolution of the O−H distances involved in the intramolecular H-bond. (c1,c2) Free-energy profile for proton transfer within the H-bond.

Sodium and potassium ions affect the symmetry of the H-bond in Hmaleate ion in different ways. Potassium ion results in a centered single-well potential energy curve, whereas sodium ion results in an asymmetric single-well potential. The strong asymmetry of the H-bond in the presence of Na^+ is not surprising, because the Na^+ repels the proton, and thus a position nearer to O1 is preferred. The surprising result is the single-well potential centered at the midpoint of the H-bond in the presence of K^+, which might have shown a greater repulsion because it is closer to the OHO.

To resolve this puzzle, the potential for H motion can again be separated into instantaneous solvation environments that favor one solvatomer or the other. We have quantified that solvation by summing the number of H-bonds between O1 or O2 of the OHO and the neighboring water hydrogens within 2.5 Å. We can thus distinguish which O is less solvated by water.

Population analysis for sodium Hmaleate in water shows that during approximately 58.3% of the simulation time oxygen atom O2 was less solvated by water than oxygen O1 and 6.8% of the time oxygen atom O1 was less solvated. For approximately 34.9%

dx.doi.org/10.1021/ct200580c |J. Chem. Theory Comput. 2011, 7, 3505–3513

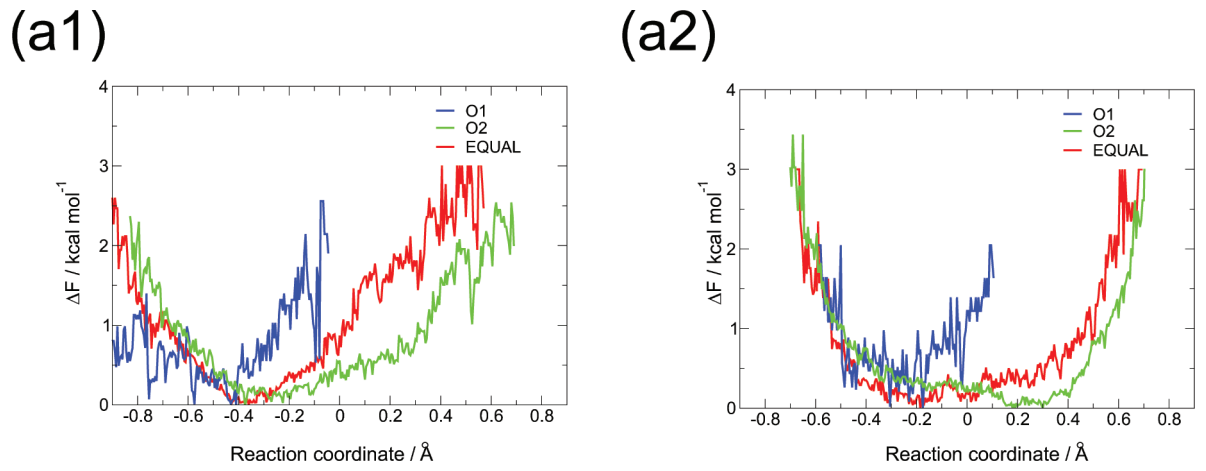

Figure 5. CPMD free-energy profiles for Hmaleate anion with Na^+ (a1) and K^+ (a2) separately for the simulation time when O1 was less solvated than O2, for the time when O2 was less solvated than O1, and for the time when both oxygen atoms were solvated similarly.

of the time, both oxygen atoms in the intramolecular H-bond were solvated more or less the same. In comparison, population analysis for potassium Hmaleate in water shows that approximately 67.9% of the simulation time oxygen atom O2 was less solvated by water than oxygen O1 and 2.3% of time oxygen atom O1 was less solvated. For approximately 29.8% of time, both oxygen atoms in the intermolecular H-bond were solvated more or less the same.

Figure 5 shows free-energy profiles for H motion in Hmaleate anion in the presence of Na^+ (a1) and K^+ (a2) from CPMD, separated into instantaneous solvation environments. For Na^+ the potential is always asymmetric, with a minimum at O1, which is farther from the sodium, regardless of the H-bonds from water. We suggest that this is because the repulsion by Na^+ is so strong that a H position nearer to O1 was always preferred. For K^+ the potential depends on the solvation by water. For the rare times when O1 was less solvated, a position for the H of the H-bond nearer to O1 was strongly preferred. In constrast, for the 67.9% of the time when O2 was less solvated, a position for the H nearer to O2 was slightly preferred, but with an energy cost of only 0.5 kcal/mol, the H could be nearer the other O, resulting in an almost symmetric potential. For the remaining time when both oxygens were solvated similarly, the potential is effectively symmetric. We suggest that these nearly symmetric potentials arise because the repulsion by the larger, more distant, and more hydrated K^+ is weaker than for Na^+ and competitive with solvation by water, so that the potential for H motion depends on the location of the K^+. Because the distribution of the K^+ is more diffuse than that of the Na^+, which is more localized between the carboxylate oxygens, the K^+ exerts a greater repulsion for the H when it is close to the OHO but a lesser repulsion when it is distant. The variable repulsion by the K^+ balances the repulsion by the waters of hydration, which depends on which O is less solvated.

Because these results for potassium ion are contrary to previous results by Lluch,[26] one should understand why? A partial explanation is that our simulations never reached a situation where either potassium or sodium ion is equidistant to both oxygen atoms of the intramolecular H-bond, which is a transition state according to Lluch's calculations. Thus we should not have been able to observe a centered proton. That is the case with sodium, but not with potassium, according to Figure 5a2, where we suggest that the centered proton arises because repulsion by the potassium ion near one carboxyl balances the repulsion by the waters of solvation on the other carboxyl.

3. CONCLUSIONS AND OUTLOOK

We have studied theoretically by means of ab initio Car−Parrinello molecular dynamics the symmetry of the intramolecular H-bond of Hmaleate anion as an isolated structure, in the crystals of its sodium and potassium salts, as a hydrated ion in water, and in water with counterions (K^+ and Na^+). The results confirm and clarify experimental findings by Perrin et al.[19]

When maleate ion is an isolated structure, molecular dynamics at 298 K predicts a truly symmetric potential with a centered proton. For two crystal structures (sodium and potassium salts) two different situations are observed. For the highly symmetric case of potassium Hmaleate, the potential is similar to that of the isolated ion, with a single-well centered proton. For sodium Hmaleate trihydrate crystal, which is of low symmetry, the different environments of the two oxygen atoms of the intramolecular H-bond of the Hmaleate result in an asymmetric single-well potential with a proton located on one oxygen atom, in agreement with the neutron diffraction study by Olovsson.[14]

Thanks to a new procedure that can produce separate free-energy profiles from periods during the simulation when one oxygen atom of the intramolecular H-bond was less well solvated than the other one and periods where both oxygen atoms were solvated to a similar extent, we have shown that the position of the proton in aqueous Hmaleate ion is entirely dependent on the solvation pattern around the oxygen atoms in the intramolecular H-bond. It is shown that the proton is always located on the oxygen atom that is less well solvated and that there is no longer a minimum at the other, better solvated oxygen.

Additionally, separation into instantaneous solvation environments has been applied to an aqueous solution of Hmaleate ion with two different counterions, namely K^+ and Na^+. Analysis of their influence on intramolecular H-bond symmetry revealed that, whereas the potential of the intramolecular H-bond in the Na^+ salt is always asymmetric, owing to strong repulsion by the Na^+ regardless of the H-bonds to water, for the K^+ salt the repulsion by this larger and more hydrated ion is weaker than for Na^+ and competitive with solvation by water, so that the potential for H motion depends on the location of the K^+.

The systems described here combine several factors that make computational studies of H-bonds difficult. First, the proton potential is highly anharmonic and fluctuating, and it is necessary to use a statistical description using molecular dynamics methods, and second, the barriers are of such height that quantum effects can be influential, as our path integral results indicate. It is very challenging to reproduce spectra of such systems. It is possible to reuse the trajectories used in this work, for example, to extract snapshots and construct their proton potential energy surfaces with the aim of further solving the vibrational Schroedinger equation and obtaining a statistically averaged vibrational spectrum.[41−43] If NMR parameters are also calculated for each point of the potential energy surface, the expectation value of the NMR shift of the proton can be obtained—such a technique was proven successful for a highly anharmonic short H-bond.[44] However, such calculations are beyond the scope of the current study.

4. METHODS

All calculations are based on ab initio molecular dynamics[45] using the efficient Car−Parrinello[46] propagation scheme as implemented in the CPMD program package.[47] These pseudopotential calculations have been carried out using the PBE[48] exchange−correlation functional within the spin-restricted Kohn−Sham formalism together with a plane-wave basis set at a kinetic energy cutoff of 100 Ry, Γ-point sampling of the Brillouin zone, and Troullier−Martins[49] norm-conserving pseudopotentials. The supercell for all these calculations was a cubic box 15 Å in length with periodic boundary conditions. All dynamic simulations were performed in the canonical ensemble at 298 K using Nosé−Hoover chain thermostats[50] in order to control the kinetic energy of the nuclei (as well as the fictitious kinetic energy of the orbitals). For the path integral case, a separate thermostat was used for each degree of freedom.[51] To account for the fact that the PBE functional tends to overstructure water compared to experiment, some researchers have conducted simulations at 400 K.[52] Nevertheless in all our simulations, we have used a proper temperature of 298 K together with long enough trajectories to avoid overly rapid proton transfer inside the intramolecular H-bond.

We have adopted the same approach as Miura et al.,[53] in which the positions of the atoms initially evolve according to the classical equations of motion. Then we proceed with PIMD simulation,[54−56] which explores the quantum behavior of both the nuclear and electronic degrees of freedom. It maps the problem of a quantum particle into one of a classical ring polymer model with beads that interact through temperature- and mass-dependent spring forces. Such mapping is known in the literature as a quantum classical isomorphism.[57−59] It should be underlined that "real" properties of the quantum systems are recovered only when the number of beads is extrapolated to infinity. The path integral simulations in the present study used eight beads and the normal mode variable transformation.[56]

A molecular dynamics time step of δt = 3 au (≈0.073 fs) was used for the integration of the Car−Parrinello equations of motion using a fictitious mass parameter for the orbitals of 400 au together with the proper atomic masses. The initial configurations were generated with classical molecular dynamics simulations of 1 ns. After this initial equilibration period (ca. 30 000 steps), the Car−Parrinello molecular dynamics simulations were performed, and the data were collected over trajectories spanning 300 000 steps (ca. 22 ps) for the sodium crystal (NaHMAL), 200 000 integration steps for the potassium crystal (KHMAL) (ca. 16 ps), 280 000 steps (ca. 20 ps) for Hmaleate ion with 103 water molecules, 250 000 steps (ca. 18 ps) for sodium Hmaleate with 102 water molecules, and 300 000 steps (ca. 22 ps) for potassium Hmaleate with 101 water molecules. Path integral runs were performed for similar time periods as the Car−Parrinello simulations.

The reaction coordinate δ is defined in eq 1 as the difference between O1−H and O2−H distances, where O1 labels the oxygen that bears the H at the beginning of the simulation and O2 labels the oxygen that is initially H-bonded to the H:

$$\delta = R_{\mathrm{O1-H}} - R_{\mathrm{O2-H}} \quad (1)$$

The reaction coordinate is a measure of the degree of proton transfer in the H-bond, with zero corresponding to the midpoint of the H-bond. Also, for the studies of counterions, the oxygen atoms involved in the H-bond are labeled as O2 for the one closer to the M^+ ion and O1 for the farther ($O1\cdots H\cdots O2\cdots M^+$). The free-energy profiles were obtained from eq 2, where k is the Boltzmann constant, N_A is the Avogadro number, T is the simulation temperature, and P is the proton distribution as a function of the reaction coordinate.

$$\Delta F = -k\cdot N_A\cdot T \ln(P(\delta)) \quad (2)$$

The visualize molecular dynamics (VMD)[60] program has been used for data visualization.

■ ASSOCIATED CONTENT

Ⓢ Supporting Information. Figures 1−4 compile free energy profiles generated for all four studied cases: standard Car−Parrinello (Figure 1) and path integral (Figure 2) simulations of hydrogen maleate ion in water and hydrogen maleate ion in water with potassium (Figure 3) and sodium (Figure 4) counterions. This material is available free of charge via the Internet at http://pubs.acs.org.

■ AUTHOR INFORMATION

Corresponding Author

*E-mail: mclar@elrond.chem.uni.wroc.pl; cperrin@ucsd.edu.

■ ACKNOWLEDGMENT

We are grateful to Jaroslaw Panek for useful discussions and to University of Wroclaw (Internal Grant for Young Scientist no. 105/10/E-344/M/2011 to P.D.) and to the U.S. National Science Foundation (grant CHE07-42801 to C.L.P.) for financial support. The calculations were carried out using resources from Wroclaw Supercomputer Center (WCSS) and the Galera-ACTION Cluster and the Academic Computer Center in Gdańsk (CI TASK).

■ REFERENCES

(1) Pimentel, G. C.; McClellan, A. L. *The Hydrogen Bond*; Freeman: San Francisco, CA, 1960.

(2) Vinogradov, S.; Linnel, R. *The Hydrogen Bond*; Van Norstrand-Reinhold: New York, 1971.

(3) *The Hydrogen Bond: Recent Developments in Theory and Experiments*; Schuster, P.; Zundel, G., Sandorfy, C.; Eds.; North-Holland: Amsterdam, The Netherlands, 1976.

(4) Warshel, A. *Biochemistry* **1981**, *20*, 3167–3177.

(5) Jeffrey, G. A.; Saenger, W. *Hydrogen Bonding in Biological Structures*; Springer: Berlin, Germany, 1991.
(6) Warshel, A. *Computer Modeling of Chemical Reactions in Enzymes and Solutions*; John Wiley & Sons: New York, 1997.
(7) Jeffrey, G. *An Introduction to Hydrogen Bonding*; Oxford University Press: Oxford, U.K., 1997.
(8) Scheiner, S. *Hydrogen Bonding: A Theoretical Perspective*; Oxford University Press: New York, 1997.
(9) Hadzi, D. *The Hydrogen Bond*; Wiley: Chichester, U.K., 1997.
(10) Desiraju, G.; Steiner, T. *The Weak Hydrogen Bond in Structural Chemistry and Biology*; Oxford Uniwersity Press: Oxford, U.K., 1999.
(11) Warshel, A. *Acc. Chem. Res.* **2002**, *35*, 385–395.
(12) Perrin, C. L. *Pure Appl. Chem.* **2009**, *81*, 571–583.
(13) Darlow, S.; Cochran, W. *Acta Crystallogr.* **1961**, *14*, 1250–1257.
(14) Olovsson, G.; Olovsson, I.; Lehmann, M. S. *Acta Crystallogr.* **1984**, *C40*, 1521–1526.
(15) Perrin, C. L.; Thoburn, J. D. *J. Am. Chem. Soc.* **1989**, *111*, 8010–8012.
(16) Perrin, C. L.; Thoburn, J. D. *J. Am. Chem. Soc.* **1992**, *114*, 8559–8565.
(17) Perrin, C. L. *Science* **1994**, *266*, 1665–1668.
(18) Mavri, J.; Hodoscek, M.; Hadzi, D. *J. Mol. Struct. (Theochem)* **1990**, *209*, 421–431.
(19) Perrin, C. L.; Nielson, J. B. *J. Am. Chem. Soc.* **1997**, *119*, 12734–12741.
(20) Perrin, C. L.; Ohta, B. K. *J. Am. Chem. Soc.* **2001**, *123*, 6520–6526.
(21) Perrin, C. L.; Ohta, B. K. *Bioorg. Chem.* **2002**, *30*, 3–15.
(22) Perrin, C. L.; Lau, J. S. *J. Am. Chem. Soc.* **2006**, *128*, 11820–11824.
(23) Perrin, C. L.; Karri, P. *Chem. Commun. (Cambridge, U. K.)* **2010**, *46*, 481–483.
(24) Perrin, C. L.; Lau, J. S.; Kim, Y.-J.; Karri, P.; Moore, C.; Rheingold, A. L. *J. Am. Chem. Soc.* **2009**, *131*, 13548–13554.
(25) Perrin, C. L.; Ohta, B. K. *J. Mol. Struct.* **2003**, *644*, 1–12.
(26) Garcia-Viloca, M.; Gonzalez-Lafont, A.; Lluch, J. M. *J. Am. Chem. Soc.* **1999**, *121*, 9198–9207.
(27) Perrin, C. L. *Acc. Chem. Res.* **2010**, *43*, 1550–1557.
(28) George, P.; Bock, C. W.; Trachtman, M. *J. Phys. Chem.* **1983**, *87*, 1839–1841.
(29) Hodoscek, M.; Hadzi, D. *J. Mol. Struct. (Theochem)* **1990**, *209*, 411–419.
(30) Garcia-Viloca, M.; Gonzalez-Lafont, n.; Lluch, J. M. *J. Am. Chem. Soc.* **1997**, *119*, 1081–1086.
(31) Bach, R. D.; Dmitrenko, O.; Glukhovtsev, M. N. *J. Am. Chem. Soc.* **2001**, *123*, 7134–7145.
(32) Woo, H.-K.; Wang, X.-B.; Wang, L.-S.; Lau, K.-C. *J. Phys. Chem. A* **2005**, *109*, 10633–10637.
(33) Ratajczak, H.; Barnes, A.; Baran, J.; Yaremko, A.; Latajka, Z.; Dopieralski, P. *J. Mol. Struct. (Theochem)* **2008**, *887*, 9–19.
(34) Wilson, C. C.; Thomas, L. H.; Morrison, C. A. *Chem. Phys. Lett.* **2003**, *381*, 102–108.
(35) Wilson, C. C.; Thomas, L. H.; Morrison, C. A. *Chem. Phys. Lett.* **2004**, *399*, 292–293.
(36) Darlow, S. *Acta Crystallogr.* **1961**, *14*, 1257–1259.
(37) Marcus, R. A. *J. Chem. Phys.* **1956**, *24*, 979–989.
(38) Borgis, D.; Hynes, J. T. *J. Chem. Phys.* **1991**, *94*, 3619–3628.
(39) Mavri, J.; Berendsen, H. J. C.; van Gunsteren, W. F. *J. Phys. Chem.* **1993**, *97*, 13469–13476.
(40) Tuckerman, M. E.; Marx, D.; Parrinello, M. *Nature* **2002**, *417*, 925–929.
(41) Pejov, L.; Spangberg, D.; Hermansson, K. *J. Phys. Chem. A* **2005**, *109*, 5144–5152.
(42) Jezierska, A.; Panek, J.; Borstnik, U.; Mavri, J.; Janezic, D. *J. Phys. Chem. B* **2007**, *111*, 5243–5248.
(43) Stare, J.; Panek, J.; Eckert, J.; Grdadolnik, J.; Mavri, J.; Hadzi, D. *J. Phys. Chem. A* **2008**, *112*, 1576–1586.
(44) Stare, J.; Jezierska, A.; Ambrozic, G.; Kosir, I. J.; Kidric, J.; Koll, A.; Mavri, J.; Hadzi, D. *J. Am. Chem. Soc.* **2004**, *126*, 4437–4443.
(45) Marx, D.; Hutter, J. *Ab Initio Molecular Dynamics: Basic Theory and Advanced Methods*; Cambridge University Press: Cambridge, U.K., 2009.
(46) Car, R.; Parrinello, M. *Phys. Rev. Lett.* **1985**, *55*, 2471–2474.
(47) Hutter, J.; et al. *CPMD Program Package*; IBM Corporation and Max-Planck Institut: Stuttgart, Germany, 1990; http://www.cpmd.org, (date accessed January 2, 2010).
(48) Perdew, J. P.; Burke, K.; Ernzerhof, M. *Phys. Rev. Lett.* **1996**, *77*, 3865–3868.
(49) Troullier, N.; Martins, J. L. *Phys. Rev. B* **1991**, *43*, 1993–2006.
(50) Martyna, G. J.; Klein, M. L.; Tuckerman, M. *J. Chem. Phys.* **1992**, *97*, 2635–2643.
(51) Tuckerman, M.; Laasonen, K.; Sprik, M.; Parrinello, M. *J. Chem. Phys.* **1995**, *99*, 5749–5752.
(52) Sit, P. H.-L.; Marziari, N. *J. Chem. Phys.* **2005**, *122*, 204510–204518.
(53) Miura, S.; Tuckerman, M.; Klein, M. *J. Chem. Phys.* **1998**, *109*, 5290–5299.
(54) Marx, D.; Parrinello, M. *Z. Phys. B* **1994**, *95*, 143–144.
(55) Marx, D.; Parrinello, M. *J. Chem. Phys.* **1996**, *104*, 4077–4082.
(56) Tuckerman, M.; Marx, D.; Klein, M.; Parrinello, M. *J. Chem. Phys.* **1996**, *104*, 5579–5588.
(57) Feynman, R.; Hibbs, A. *Quantum Mechanics and Path Integrals*; McGraw-Hill: New York, 1965.
(58) Schweizer, K.; Stratt, R.; Chandler, D.; Wolynes, P. *J. Chem. Phys.* **1981**, *75*, 1347–1369.
(59) Chandler, D.; Wolynes, P. *J. Chem. Phys.* **1981**, *74*, 4078–4095.
(60) Humphrey, W.; Dalke, A.; Schulten, K. *J. Mol. Graphics* **1996**, *14*, 33–38.